



# 1 Performance evaluation of the Alphasense OPC-N3 and 2 Plantower PMS5003 sensor in measuring dust events in the Salt 3 Lake Valley, Utah

4 Kamaljeet Kaur<sup>1</sup>, Kerry E. Kelly<sup>1</sup>

5 <sup>1</sup>Department of Chemical Engineering, University of Utah, SLC, 84102, USA

6 *Correspondence to:* Kerry Kelly (kerry.kelly@utah.edu)

7 **Abstract.** As the changing climate expands the extent of arid and semi-arid lands, the number, severity of, and health  
8 effects associated with dust events are likely to increase. However, regulatory measurements capable of capturing dust  
9 (PM<sub>10</sub>, particulate matter smaller than 10 μm in diameter) are sparse, sparser than measurements of PM<sub>2.5</sub> (PM smaller  
10 than 2.5 μm in diameter). Although low-cost sensors could supplement regulatory monitors, as numerous studies have  
11 shown for PM<sub>2.5</sub> concentration, most of these sensors are not effective at measuring PM<sub>10</sub> despite claims by sensor  
12 manufacturers. This study focuses on the Salt Lake Valley, adjacent to the Great Salt Lake, which recently reached  
13 historic lows exposing 1865 km<sup>2</sup> of dry lakebed. It evaluated the field performance of the Plantower PMS 5003, a  
14 common low-cost PM sensor, and the Alphasense OPC-N3, a promising candidate for low-cost measurement of PM<sub>10</sub>,  
15 against a federal equivalent method (FEM, beta attenuation) and research measurements (GRIMM aerosol  
16 spectrometer model 1.109) at three different locations. During a month-long field study that included five dust events  
17 in the Salt Lake Valley with PM<sub>10</sub> concentrations reaching 311 μg/m<sup>3</sup>, the OPC-N3 exhibited strong correlation with  
18 FEM PM<sub>10</sub> measurements ( $R^2 = 0.865$ , RMSE = 12.4 μg/m<sup>3</sup>) and GRIMM ( $R^2 = 0.937$ , RMSE = 17.7 μg/m<sup>3</sup>). The  
19 PMS sensor exhibited poor to moderate correlations ( $R^2 < 0.49$ , RMSE = 33-45 μg/m<sup>3</sup>) with reference/research  
20 monitors and severely underestimated the PM<sub>10</sub> concentrations (slope <0.099) for PM<sub>10</sub>. We also evaluated a PM-  
21 ratio-based correction method to improve the estimated PM<sub>10</sub> concentration from PMS sensors. After applying this  
22 method, PMS PM<sub>10</sub> concentrations correlated reasonably well with FEM measurements ( $R^2 > 0.63$ ) and GRIMM  
23 measurements ( $R^2 > 0.76$ ), and the RMSE decreased to 15-25 μg/m<sup>3</sup>. Our results suggest that it may be possible to  
24 obtain better resolved spatial estimates of PM<sub>10</sub> concentration using a combination of PMS sensors (often publicly  
25 available in communities) and measurements of PM<sub>2.5</sub> and PM<sub>10</sub>, such as those provided by FEMs, research-grade  
26 instrumentation, or the OPC-N3.

## 27 1 Introduction

28 Our changing climate is expanding the extent of arid and semi-arid lands globally; these lands currently cover  
29 approximately 1/3<sup>rd</sup> of the Earth's land surface (Williams et al., 2022; Huang et al., 2016). Recent studies suggest that  
30 this expansion of arid lands is linked to increases in the number and severity of dust events (Clifford et al., 2019; Tong  
31 et al., 2017; Ardon-Dryer and Kelley, 2022). Dust events can transport particulate matter (PM), particle-bound air  
32 toxics, and allergens over thousands of kilometers (Goudie, 2014). The suspended PM affects regional climate by



33 impacting cloud formation, precipitation processes, and convection activity (Cai et al., 2021; Kumar et al., 2021;  
34 Mallet et al., 2009). Dust events significantly affect the regional air quality (Chakravarty et al., 2021; Akinwumiju et  
35 al., 2021; Liu et al., 2020), decrease atmospheric visibility (Jayaratne et al., 2011) and have adverse effects on human  
36 health, including being linked to increased incidence of asthma, pneumonia, bronchitis, stroke, adverse birth outcomes,  
37 influenza, meningitis, and valley fever (Dastoorpoor et al., 2018; Jones, 2020; Bogan et al., 2021; Soy, 2016; Trianti  
38 et al., 2017; Diokhane et al., 2016; Schweitzer et al., 2018).

39

40 During dust events, the majority of PM is greater than 2.5  $\mu\text{m}$  in diameter (Tam et al., 2012). Government  
41 organizations, such as the World Health Organization (WHO), measure and/or provide guidelines for ambient PM<sub>10</sub>  
42 concentrations (PM<sub>10</sub>, particles with aerodynamic diameter <10  $\mu\text{m}$ ). PM smaller than 10  $\mu\text{m}$  in diameter is of  
43 particular interest because it is inhalable. The WHO has set guidelines for 24-hour and annual average PM<sub>10</sub>  
44 concentration at 45 and 15  $\mu\text{g}/\text{m}^3$ , respectively (WHO, 2022). One challenge with these 24-hour guidelines is that dust  
45 events often last a few hours, and these events are obscured when reporting only the PM<sub>10</sub> 24-hour average or  
46 comparing these averages to the 24-hour and guidelines (Ardon-Dryer and Kelley, 2022).

47

48 PM<sub>10</sub> concentrations tend to be more spatially heterogeneous than PM<sub>2.5</sub> concentrations because PM<sub>10</sub> settles more  
49 quickly (Keet et al., 2018). In addition, regulatory measurements of PM<sub>10</sub> are spatially and temporally sparser than  
50 PM<sub>2.5</sub> measurements. For example, the US EPA reports measurements from 1,370 active PM<sub>2.5</sub> sites versus 800 active  
51 PM<sub>10</sub> sites (EPA, 2022). Approximately half of these PM<sub>10</sub> sites only report 24-hour averages (USA EPA, 2022).  
52 Furthermore, many dust-prone areas of the US lack any PM monitoring (USA EPA, 2022). More highly resolved  
53 measurements of PM<sub>10</sub> concentration would aid communities and researchers in understanding and addressing the  
54 effects of windblown dust and dust events.

55

56 More recent studies of PM have leveraged low-cost PM measurements and mobile measurements to obtain higher  
57 spatial and temporal resolution PM<sub>2.5</sub> estimates (Bi et al., 2020; Caplin et al., 2019; Lim et al., 2019; Caubel et al.,  
58 2019; Kelly et al., 2021). With appropriate calibration, low-cost sensors have been demonstrated to be generally  
59 effective at measuring PM<sub>2.5</sub>; however, the most common low-cost PM sensors that employ a laser, and a photodiode  
60 to estimate particle concentration (Plantower PMS, Nova SDSS011, Sensirion SPS30, Shineyi PPD42NS, and  
61 Samyoung DSM501A) are ineffective at measuring PM<sub>10</sub> and dust (Kosmopoulos et al., 2020; Mei et al., 2020; Sayahi  
62 et al., 2019, Kuula et al. 2020) primarily due to the sensor's inability to aspirate these larger particles into the device  
63 (Ouimette et al., 2022). Kuula et al. (2020) tested several low-cost PM sensors using monodisperse di-octyl sebacate  
64 particles (0.5 – 10  $\mu\text{m}$ ) and observed a constant particle size distribution for particle sizes >0.5  $\mu\text{m}$  and indicated that  
65 these sensors are incapable of measuring coarse-mode particles (2.5-10  $\mu\text{m}$ ).

66

67 The Alphasense OPC-N series is a promising low-cost sensor for measuring PM<sub>10</sub>. It is larger and more expensive  
68 (~\$500) than many of the low-cost PM sensors (<\$50) with a greater flow rate (total flow of 5.5 LPM and sample  
69 flow rate of 0.28 L/min) and a mirror that allows collection of light scattering from broader array of angles than typical



70 low-cost PM sensors, which have flow rates on the order of 0.1 LPM (Sayahi et al., 2019; Ouimette et al., 2022;  
71 Alphasense Ltd, 2022). The OPC-N3 allows particle counting in 24-size bins for sizes ranging from 0.35–40  $\mu\text{m}$ . The  
72 working principle of Alphasense OPC-N3 and its previous version (OPC-N2) is similar to an aerosol spectrometer; it  
73 measures scattering from single particles (Vogt et al., 2021). Studies have used the Alphasense OPCs for indoor and  
74 ambient PM monitoring (Kaliszewski et al., 2020; Chu et al., 2021; Dubey et al., 2022b; Feenstra et al., 2019; Pope  
75 et al., 2018; Nor et al., 2021; Alhasa et al., 2018; Mohd Nadzir et al., 2020), to monitor  $\text{PM}_{2.5}$  personal exposure (Harr  
76 et al., 2022a), to identify PM sources (Harr et al., 2022b; Bousiotis et al., 2021), and to monitor occupational  $\text{PM}_{2.5}$   
77 and  $\text{PM}_{10}$  exposure (Runström Eden et al., 2022; Bächler et al., 2020). The Alphasense OPCs correlate well ( $R^2 =$   
78 0.93–0.99) with  $\text{PM}_{10}$  in laboratory studies (Sousan et al., 2021, 2016; Samad et al., 2021; Dubey et al., 2022a). The  
79 field-based studies have reported somewhat lower correlations ( $R^2$ : 0.53 – 0.8) (Bilek et al., 2021; Dubey et al., 2022b,  
80 a; Crilley et al., 2018), due to the variable ambient meteorological conditions and changing PM compositions. The  
81 ambient PM ratios ( $\text{PM}_{2.5}/\text{PM}_{10}$ ) in these previous studies were greater than 0.6, indicating the main contributions to  
82 PM levels were from the fine PMs, rather than coarser PMs. The ratio of  $\text{PM}_{2.5}/\text{PM}_{10}$  can provide crucial information  
83 about particle origin and formation process (Xu et al., 2017; Speranza et al., 2014). Duvall et al. (2021) have suggested  
84 evaluating the performance of  $\text{PM}_{10}$  sensors for varying  $\text{PM}_{2.5}/\text{PM}_{10}$  ratios, and dust events provide a great opportunity  
85 to evaluate  $\text{PM}_{10}$  sensor performance at ambient PM ratios  $<0.3$ .

86

87 Few studies have evaluated the performance of Alphasense OPCs for measuring  $\text{PM}_{10}$  concentration during dust  
88 events. Gomes et al. (2022) measured hourly  $\text{PM}_{10}$  concentration exceeding 300  $\mu\text{g}/\text{m}^3$  using the OPC-N3 during  
89 Saharan dust events in western Portugal. In Sarajevo, Bosnia-Herzegovina, Masic, et al. (2020) reported that for the  
90 Aralkum Desert dust event, the OPC-N2 tracked GRIMM-11D  $\text{PM}_{10}$  measurements but at a lower magnitude. Fewer  
91 studies have compared the Alphasense OPCs with the regulatory monitors during dust events. Vogt et al. (2021)  
92 reported that the OPC-N3 captures the long-range transported dust well, but slightly overestimates  $\text{PM}_{10}$  concentration  
93 ( $<120 \mu\text{g}/\text{m}^3$ ) compared to a FIDAS (EN 16450 approved regulatory instrument). They also reported a moderate  
94 correlation with  $\text{PM}_{10}$  compared to FIDAS ( $R^2 = 0.58$ – $0.64$ , and RMSE between 12–13  $\mu\text{g}/\text{m}^3$ ) and compared to a  
95 gravimetric method ( $R^2 = 0.71$ – $0.74$ , and RMSE between 9–11  $\mu\text{g}/\text{m}^3$ ). Mukherjee et al. (2017) evaluated the OPC-N2  
96 performance against a Met One beta attenuation monitor (BAM) over 12 weeks in the Cuyama Valley of California,  
97 where PM concentrations are impacted by wind-blown dust events and regional transport; they reported a moderate  
98 to good degree of correlation ( $R^2 = 0.53$ – $0.81$ , depending on sampling orientation) for  $\text{PM}_{10}$  ( $<750 \mu\text{g}/\text{m}^3$ ). In general,  
99 the studies report that the OPC-N2/N3 tracks the temporal variation of research/reference measurements but with  
100 varying correlation factors.

101

102 A high  $\text{PM}_{2.5}/\text{PM}_{10}$  ratio represents fine-dominated aerosols, likely corresponding to anthropogenic or other  
103 combustion sources. Low ratios represent coarser particles (aerodynamic size between 2.5–10  $\mu\text{m}$ ) that tend to  
104 correspond to wind-blown dust (Sugimoto et al., 2016). Sugimoto et al. (2016) classified aerosols as local dust when  
105 the  $\text{PM}_{2.5}/\text{PM}_{10}$  ratio was less than 0.1 and as transported dust when  $\text{PM}_{2.5}/\text{PM}_{10}$  ratios were between 0.1 to 0.3. During  
106 dust events, low-cost sensors like the Plantower PMSs can detect only a small portion of a particle size distribution,



107 and its response greatly depends on the particle size distribution and particle optical properties (Vogt et al., 2021).  
108 This study explores the possibility of using a size-segregated correction factor ( $PM_{2.5}/PM_{10}$  ratio) to infer  $PM_{10}$   
109 concentration from low-cost sensors that typically respond poorly to particles larger than  $2.5\ \mu\text{m}$  in diameter. If  
110 successful, this technique could leverage the large number of existing low-cost sensor measurements that use the  
111 Plantower PMS (and similar sensors) and improve spatial estimates of  $PM_{10}$  concentration.

112

113 This study aims to evaluate the Alphasense OPC-N3 to complement common low-cost PM measurements to  
114 understand  $PM_{10}$  concentrations during dust events in the Salt Lake Valley. The Salt Lake Valley is particularly well  
115 suited to studying dust events because it is affected by both regional dust events from the playas located to the west  
116 of the valley and from the drying Great Salt Lake bed, which has reached historic lows with more than  $1865\ \text{km}^2$  of  
117 exposed lakebed (Perry et al., 2019). Under appropriate meteorological conditions, portions of this exposed lakebed  
118 produce substantial dust plumes, and the winds can transport this dust directly into the populated areas of the Salt  
119 Lake Valley (Perry et al., 2019).

120

## 121 **2 Methods**

122 This study focused on April of 2022 in the Salt Lake Valley, when it experienced five dust events (summarized in  
123 Table 1). It relies on low-cost sensors and reference/research measurements at three different locations (Fig. 1): the  
124 Utah Division of Air Quality (UDAQ)'s Hawthorne monitoring station (HW), the UDAQ's Environmental Quality  
125 (EQ) station and surroundings, and a residential site (RS) in the northeast quadrant of the Salt Lake Valley. This period  
126 included an hourly average FEM (Federal Equivalent Method)  $PM_{10}$  concentration that reached  $311\ \mu\text{g}/\text{m}^3$ .



127  
128  
129  
130  
131  
132  
133  
134  
135  
136  
137  
138  
139  
140  
141  
142  
143  
144  
145  
146  
147  
148

**Figure 1:** Study locations in Salt Lake County: EQ (UDAQ Environmental Quality) site, HW (Hawthorne UDAQ) site, and RS (residential site). The distance between EQ to HW, HW to RS, and EQ to RS is 7.8 km, 4.3 km, and 7.35 km, respectively. The OPC and PMS sensors were collocated at RS and HW sites. Two PurpleAir II were located within 2 km of the EQ monitoring station.



149 **Table 1:** PM measurements at the three different study locations.

150

Site	Measurement type	Working principle	#	Sensor ID	Distance from a reference monitor	Hours of operation*
HW	OPC-N3	Light Scattering (optical particle counter)	1	OPC-HW	Collocation	633 <sup>a</sup>
	PurpleAir II	Light Scattering- (nephelometry)	2	PMS-HW-1A, PMS-HW-1B, PMS-HW-2A, PMS-HW-2B	Collocation	697
	Thermo Scientific Model 5030 SHARP analyzer	Light scattering (nephelometry) + BAM	1	PM <sub>2.5</sub> FEM-HW	Federal equivalent method	697
	MetOne E-BAM PLUS	BAM	1	PM <sub>10</sub> FEM-HW	Federal equivalent method	695
EQ	PurpleAir II	Light Scattering- (nephelometry)	2	PMS-EQ-1A, PMS-EQ-1B, PMS-EQ-2A, PMS-EQ-2B	480 m and 1.82 km	697
	Thermo Scientific Model 5030 SHARP analyzer	Light scattering (nephelometry) + BAM		PM <sub>2.5</sub> FEM-EQ	Federal equivalent method	697
	MetOne E-BAM PLUS	BAM		PM <sub>10</sub> FEM-EQ	Federal equivalent method	697
RS	OPC-N3	Light Scattering (optical particle counter)	1	OPC-RS	Collocation	425 <sup>c</sup>
	PurpleAir II	Light Scattering- (nephelometry)	2	PMS-RS-1A, PMS-RS-1B, PMS-RS-2A, PMS-RS-2B	Collocation	302 <sup>d</sup>
	GRIMM 1.109	Light Scattering (optical particle counter)		GRIMM	Research monitor	452

151 <sup>a</sup>Total number of hours = 711. Measurements corresponding to relative humidity >85%, i.e., 14 hrs, were  
 152 excluded.

153 <sup>b</sup>OPC-HW measurements were not available between 4/12/2022 6:00 pm – 4/14/2022 7:00 pm due to connectivity  
 154 issues.

155 <sup>c</sup>The measurements for OPC-RS were available starting 9 April 2022. OPC-RS measurements between 4/14/2022  
 156 10:00 am – 4/17/2022 20:00 pm were not available due to connectivity issues.

157 <sup>d</sup>The measurements from all the PurpleAir II at RS were available starting on 18 April 2022

158



## 159 2.1 Low-cost sensors

160 The low-cost sensors tested in this study include the Alphasense optical particle counter (OPC-N3, Alphasense Ltd,  
161 \$500) and the Plantower PMS5003 (\$20) integrated into the PurpleAir II (~\$259). The Alphasense OPC-N3 uses a  
162 class 1 laser (~658 nm) to detect, size, and count particles in the size range 0.35-40  $\mu\text{m}$  in 24 bins, which is translated,  
163 using the embedded algorithm, into estimated  $\text{PM}_{10}$ ,  $\text{PM}_{2.5}$ , and  $\text{PM}_1$  mass concentrations. The default setting for the  
164 OPC-N3's refractive index is 1.5 (real part) and for density is 1.65  $\text{g}/\text{cm}^3$ , and these default settings were used  
165 throughout this study. The OPC-N3 uses an internal fan to create flow and reports a sample flow rate (~0.28 L/min  
166 and a total flow rate of 5.5 LPM). Each OPC-N3 was connected to a laptop and used the manufacturer-provided  
167 software. The OPC-N3 was set to store measurements every 1 min. The measurements included the date, size bins  
168 and counts, pump flow, relative humidity (RH), temperature, and  $\text{PM}_1$ ,  $\text{PM}_{2.5}$ , and  $\text{PM}_{10}$  concentration.

169

170 The PMS 5003 is a low-cost sensor (~\$20, Plantower Technology, China), which has been integrated into a variety of  
171 low-cost air quality sensor packages, such as TSI BlueSky, PurpleAir, etc. It uses a fan to create a flow (~0.1 L/min),  
172 and it is equipped with a red laser (~680  $\pm$  10 nm), a scattering angle of 90°, and a photo-diode detector to convert  
173 the scattered light to a voltage pulse (Sayahi et al., 2019; Ouimette et al. 2022). The PMS sensor converts light scattering  
174 into several different air quality parameters, including particle counts (0.3-10  $\mu\text{m}$ ),  $\text{PM}_{10}$ ,  $\text{PM}_{2.5}$ , and  $\text{PM}_1$ , although  
175 these different metrics are all based on this single measurement, total light scattering. The PMS 5003 has been  
176 evaluated extensively in the laboratory and the field, and the measurements tend to correlate well with  $\text{PM}_{10}$  or  $\text{PM}_{2.5}$   
177 concentration although it performs poorly for larger PM sizes, such as  $\text{PM}_{2.5}$  -  $\text{PM}_{10}$  (Sayahi et al., 2019; Vogt et al.,  
178 2021; Kuula et al., 2020; Ouimette et al., 2022). In this study, we used two PurpleAir PA-II at the HW and RS sites,  
179 each PA-II has two PMS sensors per node.  $\text{PM}_{10}$  mass concentration corresponding to correction factor (CF) =1 and  
180 a data collection rate of every 2 minutes were used. The data were downloaded from the PurpleAir website. In addition,  
181 we evaluated two PurpleAir PA-II sensors located within 2 km of the EQ monitoring station.

182 All the OPC-N3 were placed inside a custom build housing to protect the sensor from rain and insects. The details of  
183 housing can be found in the supplementary material (Section S3).

184

## 185 2.2 Site descriptions

186 The study includes measurements from the two UDAQ sites (HW and EQ) in Salt Lake County that provide both  
187 hourly  $\text{PM}_{2.5}$  and  $\text{PM}_{10}$  measurements (Fig. 1). UDAQ uses a Thermo Scientific Model 5030 SHARP analyzer for  
188 measuring hourly  $\text{PM}_{2.5}$  concentration and a MetOne E-BAM (Beta Attenuation Monitoring) PLUS for measuring  
189  $\text{PM}_{10}$  concentration. We placed two PurpleAir PA-II (containing four Plantower PMS 5003s, named: PMS-HW-1A,  
190 PMS-HW-1B, PMS-HW-2A, PMS-HW-2B) and one OPC-N3 (named: OPC-HW) at the HW site (Table 1). The  
191 PurpleAir PA-IIs and the OPC-N3 were mounted on poles that extend above the roof of the HW monitoring station.  
192 The HW monitoring station is located in an urban residential area (AQS: 49-035-3006, Lat: 40.7343, Long: -111.8721)  
193 at an elevation of 1308m. This site was established to represent population exposure in the Salt Lake City area, and it  
194 is often the controlling monitor for the county. The average of PMS-HW-1A, PMS-HW-2A, and PMS-HW-2B  $\text{PM}_{10}$



195 concentrations at HW were named PMS-HW. PMS-HW-2B was excluded from the PMS-HW average because of its  
196 moderate correlation with the other three sensors (Fig. S2).

197

198 We also evaluated two PurpleAir II (containing four Plantower PMS 5003s, named PMS-EQ-1A, PMS-EQ-1B, PMS-  
199 EQ-2A, PMS-EQ-2B) sensors located near the UDAQ EQ site. One of the sensors was 480 m away (PMS-EQ-1),  
200 while the other was 1.82 km away (PMS-EQ-2). The EQ monitoring station (AQS: 49-035-3015, Lat: 40.777028,  
201 Long: -111.94585, elevation 1284 m) is located approximately 14 km southeast of the Great Salt Lake dry lake bed.  
202 In addition to PM concentrations, we accessed relative humidity (RH), temperature, wind speed, and wind direction  
203 data from the two UDAQ monitoring sites on EPA's AirNow Tech website. EPA-flagged measurements were  
204 excluded from this study. UDAQ uses RM Young Ultrasonic Anemometer Model 86004 to measure the wind speed  
205 and wind direction and an instrument based on a hygroscopic plastic film to measure relative humidity.

206

207 The RS was located in the northeast quadrant of the Salt Lake Valley at an elevation of 1383 m (40.771938, -  
208 111.861290). Measurements at this site included four Plantower PMS 5003s (labeled as PMS-RS-1A, PMS-RS1B,  
209 PMS-RS-2A, PMS-RS-2B) in two PurpleAir PA-IIs, one OPC-N3 (labeled as OPC-RS) and one GRIMM (model  
210 1.109 Aerosol Technik Ainring, Germany). The GRIMM employs an internal pump to create a flow of 1.2 L/min and  
211 measures the number concentration of particles of size 0.265  $\mu\text{m}$  – 34  $\mu\text{m}$  in 31 size bins, and reports estimated PM<sub>1</sub>,  
212 PM<sub>2.5</sub>, and PM<sub>10</sub> concentrations. The GRIMM measurements were stored every minute in an internal storage card.  
213 The GRIMM measurements were not available between 4/24/2022 6:00PM -4/26/2022 2:00 PM MDT (Mountain Day  
214 Time). The PurpleAir PA-IIs and the GRIMM were mounted on the east side of a small outbuilding.

215

### 216 **2.3 Data Analysis**

217 The measurements from the low-cost sensors and the research monitor (GRIMM) were converted to hourly average  
218 concentrations and time-synchronized to MDT. Two EPA-flagged measurements corresponding to unexplainable high  
219 hourly PM<sub>10</sub> concentrations (>800  $\mu\text{g}/\text{m}^3$ ) from FEM-HW were removed. The low-cost sensors used in this study were  
220 not supplemented with dryers, and therefore their performance is affected by high humidity conditions, which can  
221 result in condensation and droplet formation (Samad et al., 2021). Consequently, the measurements corresponding to  
222 relative humidity greater than 85% were excluded from the study (<2% of total measurements).

223

224 Using the HW and EQ meteorological measurements, we defined dust events as periods with PM<sub>10</sub> concentrations  
225 exceeding 100  $\mu\text{g}/\text{m}^3$  accompanied by winds exceeding 5 m/s at either site. These high winds were either observed at  
226 the beginning or during dust events. Each dust event typically included a period of time when PM<sub>10</sub> concentrations  
227 began increasing before reaching peak values. After wind speeds began to decrease, PM<sub>10</sub> concentration decreased  
228 gradually. The dust events in this study included the entire time period when wind/PM<sub>10</sub> levels decreased until PM<sub>10</sub>  
229 concentrations reached background levels (<50  $\mu\text{g}/\text{m}^3$ ). Table 2 (for HW) and Table 1S (for EQ) provide the



230 meteorological parameters (wind speed, wind direction, temperature, and RH), PM<sub>2.5</sub> and PM<sub>10</sub> concentrations, and  
231 PM<sub>2.5</sub>/PM<sub>10</sub> ratios for each event.

232

233 We performed a linear regression to relate the PM<sub>10</sub> concentration measurements of the low-cost sensors to reference  
234 monitors at HW and EQ and a research monitor at the RS. Performance guidelines for low-cost PM<sub>10</sub> measurements  
235 are not yet available. For discussion purposes, we use EPA guidelines for low-cost PM<sub>2.5</sub> sensors, which include  
236 acceptable performance as a slope of  $1 \pm 0.35$ , intercept of  $0 \pm 5 \mu\text{g}/\text{m}^3$ , root mean square error (RMSE)  $\leq 7 \mu\text{g}/\text{m}^3$ ,  
237 normalized root mean square error (NRMSE)  $\leq 30\%$ , and  $R^2 > 0.7$  (when compared with the reference monitor)  
238 (Rachelle M. Duvall et al., 2021). RMSE and NRMSE were calculated using the following equations:

$$239 \quad RMSE = \sqrt{\frac{1}{N} \sum_{t=1}^N (low\ cost\ sensor_t - Ref_t)^2}$$

$$240 \quad NRMSE = \frac{RMSE}{\overline{Ref}} \times 100$$

241 where, *low cost sensor* represents the low-cost sensor measurement,  $\overline{Ref}$  represents the reference/regulatory  
242 measurements, and  $\overline{Ref}$  represents the average of the reference or regulatory monitor measurements.

243

244 We also explored a PM<sub>2.5</sub>/PM<sub>10</sub> ratio-based calibration strategy for correcting PMS sensor readings. Based on the ratio  
245 of FEM-HW PM<sub>2.5</sub>/PM<sub>10</sub>, we segregated the FEM-HW and PMS-HW PM<sub>10</sub> measurements into six bins: PM<sub>2.5</sub>/PM<sub>10</sub>:  
246  $<0.2$ ,  $0.2-0.3$ ,  $0.3-0.4$ ,  $0.4-0.5$ ,  $0.5-0.7$ , and  $>0.7$ . For each bin, the co-located PMS-HW PM<sub>10</sub> concentrations were  
247 linearly regressed against the FEM-HW PM<sub>10</sub> concentrations to obtain correction factors (slope and intercept). These  
248 correction factors were later used to correct the PMS PM<sub>10</sub> concentrations at the other two locations (RS and EQ). The  
249 PM<sub>2.5</sub>/PM<sub>10</sub> ratios from the GRIMM and OPC-RS at the RS were calculated for use in the in selecting the appropriate  
250 PM-ratio-based correction factor and subsequent correction of the collocated PMS sensors. At the EQ site, the  
251 PM<sub>2.5</sub>/PM<sub>10</sub> ratio from the FEM-EQ was used to select the appropriate PM-ratio-based correction factor and  
252 subsequent correction of the nearby PMS sensors.

253

254



255 **Table 2:** Meteorological and PM characteristics during the dust events at the HW monitoring site. The number in the parenthesis  
 256 represents the minimum and maximum of the parameter. Parameters for the EQ site can be found in Table S1 (supplementary  
 257 material).

Start	Duration (hr)	Wind Speed (m/s)	Relative humidity %	Temperature (°C)	PM <sub>2.5</sub> /PM <sub>10</sub>	PM <sub>10</sub> (µg/m <sup>3</sup> )
4/9/22 5:00 AM	7	3.13 [1.13, 4.16]*	37.9 [28, 46]	10.4 [8.3, 13.8]	0.14 [0.10, 0.27]	81.3 [36, 140]
4/11/22 10:00 AM	9	4.12 [2.11, 5.91]	20.9 [12, 37]	12.4 [7.2, 15.6]	0.2 [0.13, 0.36]	67.6 [44, 101]
4/19/22 9:00 AM	10	3.75 [1.64, 5.60]	23.4 [17,32]	16.7 [13.3, 18.3]	0.24 [0.13, 0.36]	96.5 [54, 161]
4/21/22 11:00 AM	23	3.54 [1.02, 6.73]	37.6 [10, 79]	15.6 [7.2,23.9]	0.15 [0.08, 0.24]	141 [51, 274]
4/28/22 9:00 PM	4	3.17 [1.54, 5.14]	36.5 [28, 45]	14.4 [11.1, 17.2]	0.2 [0.10, 0.38]	79.5 [26, 128]

258 \*a wind speed of 6.27 m/s was observed at the EQ site

259

### 260 3 Results and Discussion

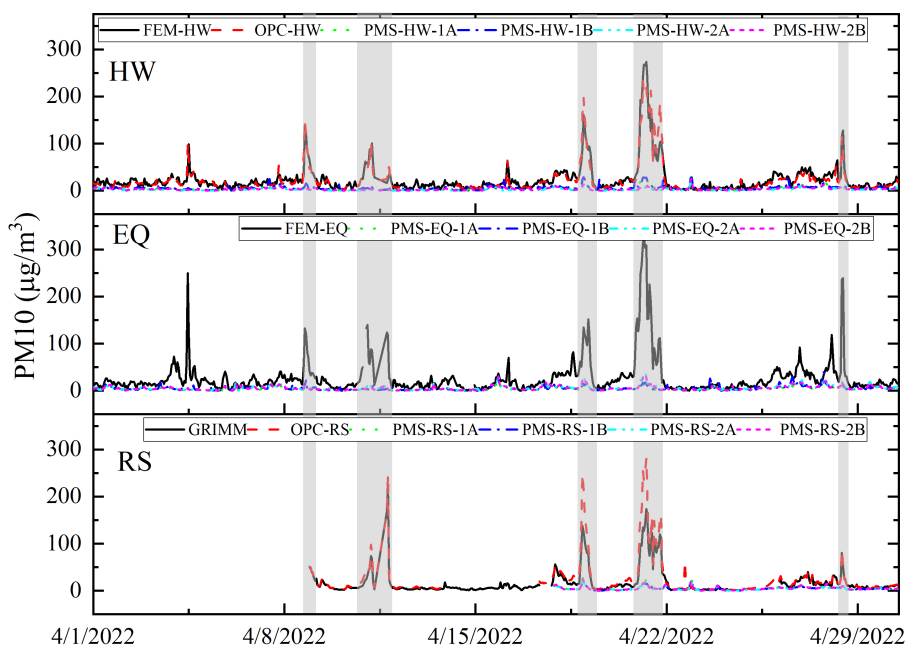
261 Figure 2 shows the hourly average PM<sub>10</sub> concentration at the three different sites, with the dust events highlighted in  
 262 grey. The five dust events were observed at all three locations, and they occurred at approximately the same time.  
 263 Four of the dust events lasted less than 10 hours, and the event on 21 April 2022 lasted 23 hours. The PM<sub>2.5</sub>/PM<sub>10</sub> ratio  
 264 (Table 1) remained less than 0.3 during all the events, indicating the predominant contribution of coarser particles to  
 265 PM<sub>10</sub>. For each event, the PM<sub>10</sub> concentrations reached at least 100 µg/m<sup>3</sup>. During the 21<sup>st</sup> April event, hourly average  
 266 PM<sub>10</sub> concentrations reached 275 µg/m<sup>3</sup> at HW, 311 µg/m<sup>3</sup> at EQ, and 173 µg/m<sup>3</sup> at the RS site (Table 1 and Table  
 267 1S). The lower PM<sub>10</sub> concentration at the RS may be due to its residential location, its higher altitude, and its greater  
 268 distance from dust sources. The OPC-HW and OPC-RS PM<sub>10</sub> concentration estimates followed the temporal pattern  
 269 of the reference/research monitors including during the dust events. Previous studies have observed similar response  
 270 for OPC-N3 and OPC-N2 (previous version of the OPC-N3) for dust events (Masic et al., 2020; Vogt et al., 2021).  
 271 Vogt et al. (2021) found that the OPC-N3 tracked PM<sub>10</sub> concentrations from a FIDAS (EN 16450 approved regulatory  
 272 instrument) for long-range transport dust events (PM<sub>10</sub> range 60 – 125 µg/m<sup>3</sup>). The PMS sensors followed the temporal  
 273 pattern of the reference/research monitors except during the dust events when the PMS sensors substantially  
 274 underestimated PM<sub>10</sub> concentration (Fig. 2). Vogt et al. (2021) also found that the PMS5003 underestimated the PM<sub>10</sub>  
 275 concentration during dust events. In addition, Masic et al. (2020) reported that during the Aralkum Desert dust event  
 276 (PM<sub>10</sub> reached 160 µg/m<sup>3</sup>), the PM<sub>10</sub> reported by OPC-N2 agreed well with the GRIMM 11-D (research-grade optical  
 277 particle sizer), whereas the PMS5003 was not able to detect a large fraction of coarse particles correctly. Most of these



278 studies recorded one dust event during their sampling duration, whereas this study found that the OPC-N3 tracked  
279 multiple dust events.

280

281 Figure 3 shows wind roses for April 2022 and each of the dust events. During the month of April, winds exceeding 5  
282 m/s were observed at HW during 2.5% of the hours (1.81 % south predominant and 0.69% west predominant). For  
283 dust events observed on 11<sup>th</sup> April and 21-22<sup>nd</sup> April, the high winds came from the south, whereas, for the rest of the  
284 events, high winds predominantly came from the west. The different wind directions could be transporting dust from  
285 different sources, such as the playas to the south and west of the Salt Lake Valley, the exposed playas of the Great  
286 Salt Lake, or local sources, such as mine tailing, gravel operations, unpaved roads, and an open-pit copper mine  
287 (Hahnenberger and Nicoll, 2012; Perry et al., 2019). All study monitoring sites are located west and southwest of the  
288 Great Salt Lake (Perry et al., 2019). Identifying the sources of the wind-blown dust and the effects of these differences  
289 on sensor performance would require a thorough analysis of the meteorology, the PM composition, and size  
290 distribution during the study period.



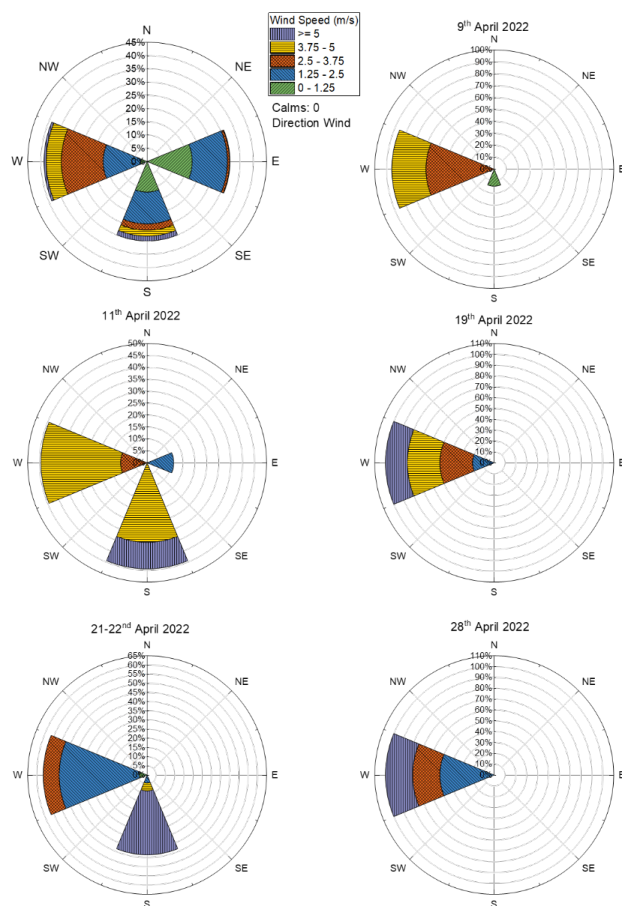
291  
292 **Figure 2:** Hourly averaged PM<sub>10</sub> concentrations from the FEM, research monitors and low-cost sensors at the three different sites:  
293 HW, EQ, and RS. Black solid lines represent reference/research monitors; red dash represents OPC-N3; green dot, blue dash-dot,  
294 turquoise dash-dot-dot, and pink short-dash represent PMS sensors. The shaded peaks on 4/9/2022, 4/11/2022, 4/19/2022,  
295 4/21/2022, and 4/28/2022 correspond to dust events. More details on these events can be found in Table 2.

296



297 **3.1 OPC-N3 performance**

298 Figure 4 illustrates the strong correlation between the OPC-N3 and the PM<sub>10</sub> concentration measured by the FEM at  
299 the HW site and the GRIMM monitor at the RS where the coefficient of determination ranges from 0.865 and 0.937.  
300 The intercept, slope, and R<sup>2</sup> were within the guidelines suggested by the EPA for low-cost PM<sub>2.5</sub> sensors, although the  
301 RMSE and NRMSE (uncorrected measurements) exceeded the guidelines, 12.4 µg/m<sup>3</sup> and 53.5 %, respectively (Fig.  
302 4). Vogt et al. (2021) also observed a similar slope (0.84-0.9 µg/m<sup>3</sup>) and RMSE (12-13 µg/m<sup>3</sup>) for OPC-N3 hourly  
303 PM<sub>10</sub> compared to FIDAS, but with a lower correlation (R<sup>2</sup> 0.58-0.64) and for lower concentrations than this study.  
304 Vogt et al. (2021) did not correct the PM<sub>10</sub> measurements for relative humidity, and approximately 20–30% of their  
305 measurements corresponded to high humidity conditions (RH >85%), and the inclusion of elevated RH conditions  
306 may have affected their correlations. The coefficient of determination in this study dropped to 0.81 after the inclusion  
307 of measurements corresponding to RH above 85%, which corresponded to just 2% of the total measurements (Fig.  
308 S1). Mukherjee et al. (2017) also reported correlations as high as 0.81 for OPC-N2 compared to BAM PM<sub>10</sub>  
309 measurements in the Cuyama Valley of California, with OPC-N2 reporting PM<sub>10</sub> concentrations of as high as 750  
310 µg/m<sup>3</sup>. Mukherjee et al. (2017) also did not correct the OPC data for relative humidity, which may have affected their  
311 correlations. Our study as well as previous studies suggest that the OPC-N3/OPC-N2 tends to underestimate the PM<sub>10</sub>  
312 concentrations compared to the BAM (Mukherjee et al., 2017; Imami et al., 2022). The operating principle of the  
313 BAM and OPC-N3 differ. The BAM PM<sub>10</sub> measurements are based on beta attenuation and do not require assumptions  
314 about particle properties or particle size distribution. In contrast, OPCs rely on the measured particle size distribution  
315 and assumed or measured particle properties (i.e., refractive index, shape, and density that can be size dependent) to  
316 estimate mass concentration. In addition, particles < 0.3 µm in diameter do not scatter light sufficiently. Consequently,  
317 some deviation from the mass measured by the FEM is expected. The assumptions about refractive index and shape  
318 affect how particles are size classified, and in addition assumptions about density, affect estimates of mass  
319 concentration.



320

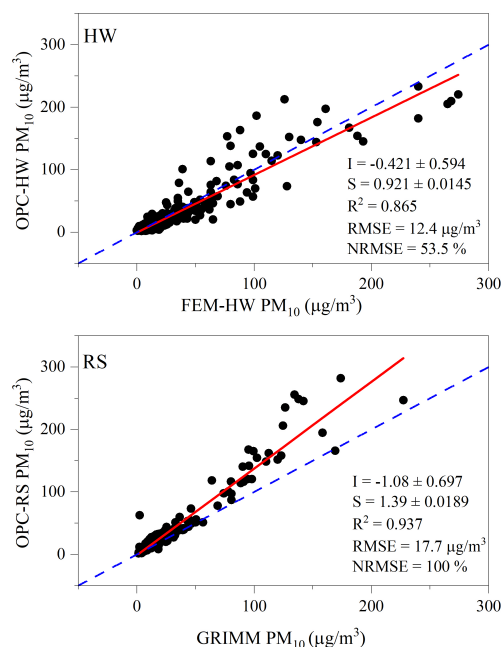
321 **Figure 3:** Wind roses for April 2022 and individual dust events, observed at HW. The wind roses for the EQ site can be found in  
322 the supplementary material (Fig. S13).

323

324 At the RS site, the OPC-RS showed a strong correlation with the GRIMM ( $R^2 > 0.9$ ) and somewhat overestimated the  
325  $PM_{10}$  concentration (slope = 1.45) compared to the GRIMM's default settings (Fig. 4). Such behavior from OPC-N3  
326 and its predecessor model OPC-N2 has been observed previously. Crilley et al. (2018) also observed this same  
327 behavior for  $PM_{10}$  for the OPC-N2 versus the GRIMM (1.108) and reported that the OPC-N2 estimated two to five  
328 times greater  $PM_{10}$  mass than the GRIMM. Sousan et al. (2016) observed a slope of 1.6 for the Alphasense OPC-N2  
329 compared to a GRIMM (1.108) for Arizona Road Dust. They attributed this behavior to the higher detection efficiency  
330 of OPC-N2 for particles  $> 0.8 \mu m$  compared to the GRIMM, and the effect of aerosol composition on OPC-N2  
331 readings. Unlike Sousan et al. (2016), Bezantakos et al. (2018), using polystyrene spheres (size: 0.8, 1, 2.5, 5.1, 7.2,  
332 and  $10.2 \mu m$ ), reported that the OPC-N2 overestimated particle number concentrations, compared to GRIMM (1.109),  
333 for all sizes, not just size  $> 1 \mu m$ .



334  
335 Crilley et al.(2018) considered high relative humidity as a controlling factor behind the overestimation by the OPC-  
336 N2. Badura et al. (2018) also reported a strong effect of relative humidity on the OPC-N2 measurements. We excluded  
337 measurement corresponding to  $RH > 85\%$  because we focus on dust events, and RH is low during these events. We  
338 investigated the effect of RH (after excluding values  $> 85\%$ ) by performing a multilinear regression with the FEM-  
339 HW as the dependent variable and the OPC-HW  $PM_{10}$  concentration and RH as independent variables. Adding RH  
340 did not significantly improve the correlation coefficient (not including RH:  $R^2 = 0.865$ ,  $RMSE = 12 \mu\text{g}/\text{m}^3$ ; including  
341 RH:  $R^2 = 0.872$ ,  $RMSE = 11.7 \mu\text{g}/\text{m}^3$ ; Section S1, Supplementary material). Hygroscopic growth changes with PM  
342 composition (Masic et al. 2020), and correcting measurements using a constant humidity coefficient can inject noise  
343 into the results. In addition, the Salt Lake Valley is in an arid region, and 82% of PM measurements corresponded to  
344 an RH of less than 60%. Consequently, the measurements were not corrected for the relative humidity for this study.



345  
346 **Figure 4:**  $PM_{10}$  concentration (top) OPC-HW vs. FEM-HW  $PM_{10}$  concentration for the period between 04/1/2022-04/30/2022,  
347 (bottom) OPC-RS vs. GRIMM  $PM_{10}$  concentration at the RS for the sampling period 04/09/2022-04/30/2022. The red solid line  
348 represents linear fit, and the blue dashed line represents the 1:1 line. I: intercept; S: slope.

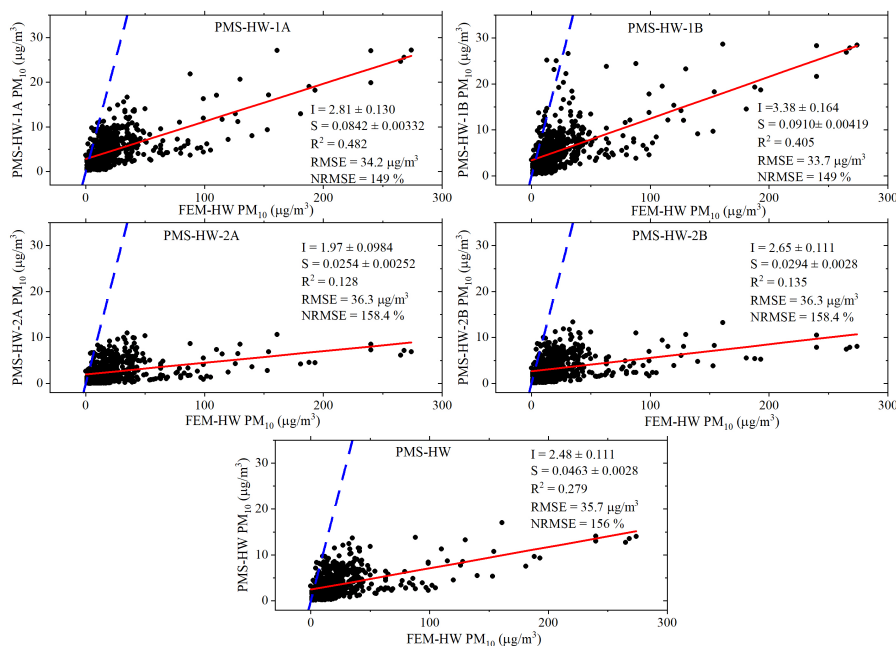
349

### 350 3.2 Performance of the PMS5003

351 Figure 5, Figure 7 (top), and Figure 8 (top) illustrate the PMS sensors' poor-to-moderate correlations ( $R^2$  between  
352 0.128 and 0.482) with reference/research measurements of  $PM_{10}$  concentration; these sensors underestimate the  $PM_{10}$   
353 concentration (slope  $< 0.09$ ), particularly during dust events. These sensors also show high RMSEs ( $> 30 \mu\text{g}/\text{m}^3$ ). Poor



354 performance of PMS sensors for PM<sub>10</sub> has been reported previously (Masic et al., 2020; Sayahi et al., 2019). Unlike  
355 the OPC-N3, PMS sensors are nephelometers (Ouimette et al., 2022) and not optical particle counters, and their  
356 response decreases with increasing size. Previous studies reported decreased response from PMS 5003 sensors for  
357 particles larger than 0.5 μm (He et al., 2020; Kuula et al., 2020; Tryner et al., 2020). Kuula et al. (2020) and Tryner et  
358 al. (2020) observed constant particle size distributions from the PMS 5003 regardless of actual particle size (exposed  
359 monodisperse particles from polystyrene latex spheres, 0.1 – 2 μm, or generated with di-octyl sebacate 0.5– 10 μm).  
360 The PMS sensors' inability to aspirate particles larger 2.5 μm is a significant cause of these sensors' inability to detect  
361 coarse particles (aerodynamic size between 2.5 – 10 μm), such as those that dominate dust events (Ouimette et al.  
362 2021).  
363



364  
365 **Figure 5:** PMS PM<sub>10</sub> concentration vs. FEM-HW PM<sub>10</sub> concentration. PMS-HW represents the average of three PMS sensors  
366 (PMS-HW-1A, PMS-HW-2A, and PMS-HW-2B). The red solid line represents linear fit, and the blue line represents the 1:1 line.  
367 The plot includes measurements recorded between 04/1/2022 – 04/30/2022. I: intercept, and S: slope.

368  
369 The PMS sensors also exhibited some inter-sensor variability during this study (Fig. S2). One sensor, PMS-HW-1B,  
370 exhibited a fair correlation with the other three PMS sensors ( $R^2 = 0.53$ - $0.55$  with slopes differing by more than 50%).  
371 The remaining three sensors (when compared to each other) had  $R^2$  greater than 0.7, although their slopes differed by  
372 40% (slope: PMS-HW-2A vs. PMS-HW-1A = 0.504; PMS-HW-2B vs PMS-HW-1A = 0.577). In terms of response



373 to  $PM_{10}$  and correlation with the reference monitor, PMS-HW-1(A and B) performed somewhat better than PMS-HW-  
374 2 (A and B) ( $RMSE < 35 \mu g/m^3$  and  $R^2 > 0.4$ , compared to  $RMSE < 36$  and  $R^2 > 0.15$ ).

375

376 Sensor-to-sensor variability has been reported in previous studies of PMS sensors, particularly for  $PM_{2.5}$  concentration  
377 (Sayahi et al., 2019; Tagle et al., 2020). The two PurpleAir II sensors (four PMS sensors) at the HW site were deployed  
378 on different dates. PMS-HW-1 was deployed on 4/24/2020, whereas the PMS-HW-2 was deployed on 9/20/2019.  
379 These sensors could be from different manufacturing batches, and they experienced different amounts of time in the  
380 field. Sensor aging can cause differences in PMS sensor performance (Tryner et al., 2020). In addition, because the  
381 PMS sensors are inefficient at measuring particles larger than  $PM_{2.5} \mu m$  in diameter, as evidenced by the low slopes  
382 in Figure 5, small differences (potentially due to sensor orientation and inherent differences in the sensors themselves)  
383 can magnify sensor to sensor variability. Mukherjee et al. (2017) and Duvall et al. (2021) discuss the importance of  
384 sampler positioning for  $PM_{10}$  measurements. For presentation purposes, we have excluded the PMS-HW-1B, which  
385 exhibited poor correlation with the other PMS sensors (PMS-HW-1A, PMS-HW-2A, and PMS-HW-2B), and  
386 averaged the remaining three PMS  $PM_{10}$  concentrations at HW and compared the average of the three sensors to the  
387  $PM_{10}$  concentrations measured by the FEM. Figure 5 shows the poor  $R^2$  between the average of all PMS sensors and  
388 FEM  $PM_{10}$  ( $R^2 = 0.279$ ), and how the PMS-HW underestimates the  $PM_{10}$  composition (slope of 0.0463).

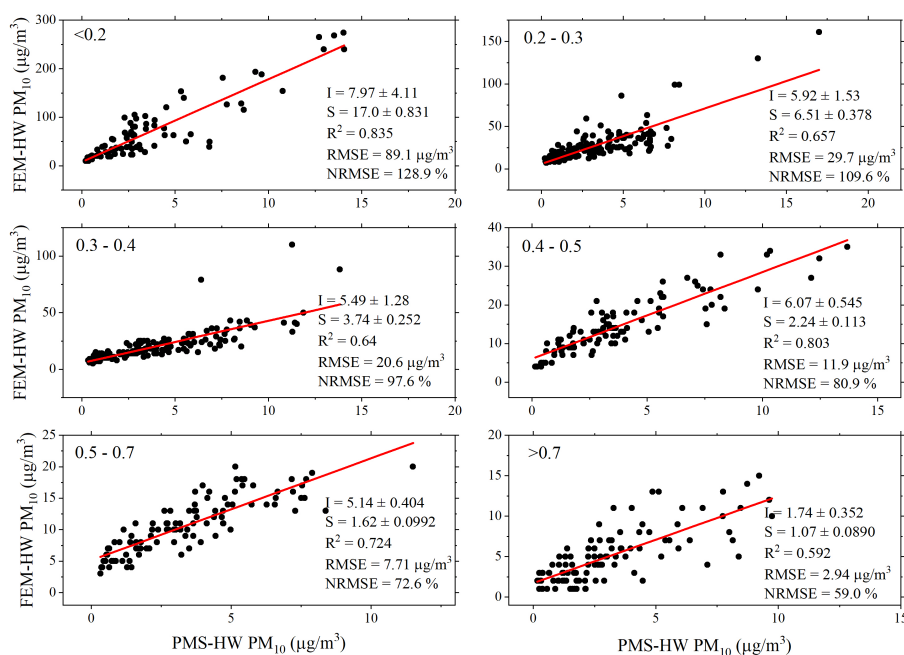
389

### 390 **3.3 Using $PM_{2.5}/PM_{10}$ ratios to obtain size-segregated PMS correction factors**

391 The effect of correcting the PMS measurements with  $PM_{2.5}/PM_{10}$  ratio-based factors on PMS performance was  
392 explored as a strategy to obtain correction factors that could enable the PMS measurements to infer  $PM_{10}$   
393 concentrations. The  $PM_{2.5}/PM_{10}$  ratio, calculated using the  $PM_{2.5}$  and  $PM_{10}$  concentrations reported by the FEM-HW,  
394 was used to segregate the PMS-HW measurements into six bins:  $PM_{2.5}/PM_{10}$ :  $<0.2$ ,  $0.2-0.3$ ,  $0.3-0.4$ ,  $0.4-0.5$ ,  $0.5-0.7$ ,  
395  $>0.7$ . For all the binned ratios (Figure 6), the PMS showed a consistent  $R^2$  of greater than 0.6 (compared to  $R^2$  values  
396 of  $0.128 - 0.482$  prior to binning), but with very different slopes for the different  $PM_{2.5}/PM_{10}$  bins. The slope varied  
397 between  $17 - 1.07$ , with the magnitude decreasing with the  $PM_{2.5}/PM_{10}$  ratio. Note that Figures 4 and 5 show the FEM  
398 on the x axes, whereas Figure 6 shows the regression equations used for correcting the PMS measurements (with FEM  
399 on the y axes). During the dust events, the  $PM_{2.5}/PM_{10}$  ratio was less than 0.3, supporting the large contribution from  
400 dust and the corresponding large magnitude of  $PM_{10}$  concentration. The  $PM_{10}$  concentrations were lowest for the high  
401  $PM_{2.5}/PM_{10}$  ratios ( $>0.7$ ), and most  $PM_{10}$  concentrations were below  $5 \mu g/m^3$ , which is close to the BAM's lower limit  
402 of detection (Met One Technical Bulletin BAM-1020 Detection Limit, 2022) and likely contributes to the low  
403 correlation observed for this ratio.

404

405 The slope and intercept for each bin were used as correction factors, called PM-ratio-based correction factors, to  
406 correct the PMS  $PM_{10}$  measurements at the other two locations, i.e., RS and EQ.



407  
408 **Figure 6:** PMS-HW PM<sub>10</sub> concentration (average of three PMS sensors at HW) vs. FEM-HW PM<sub>10</sub> concentration for different  
409 PM<sub>2.5</sub>/PM<sub>10</sub> bins. The RMSE and NRMSE has units μg/m<sup>3</sup> and %, respectively.

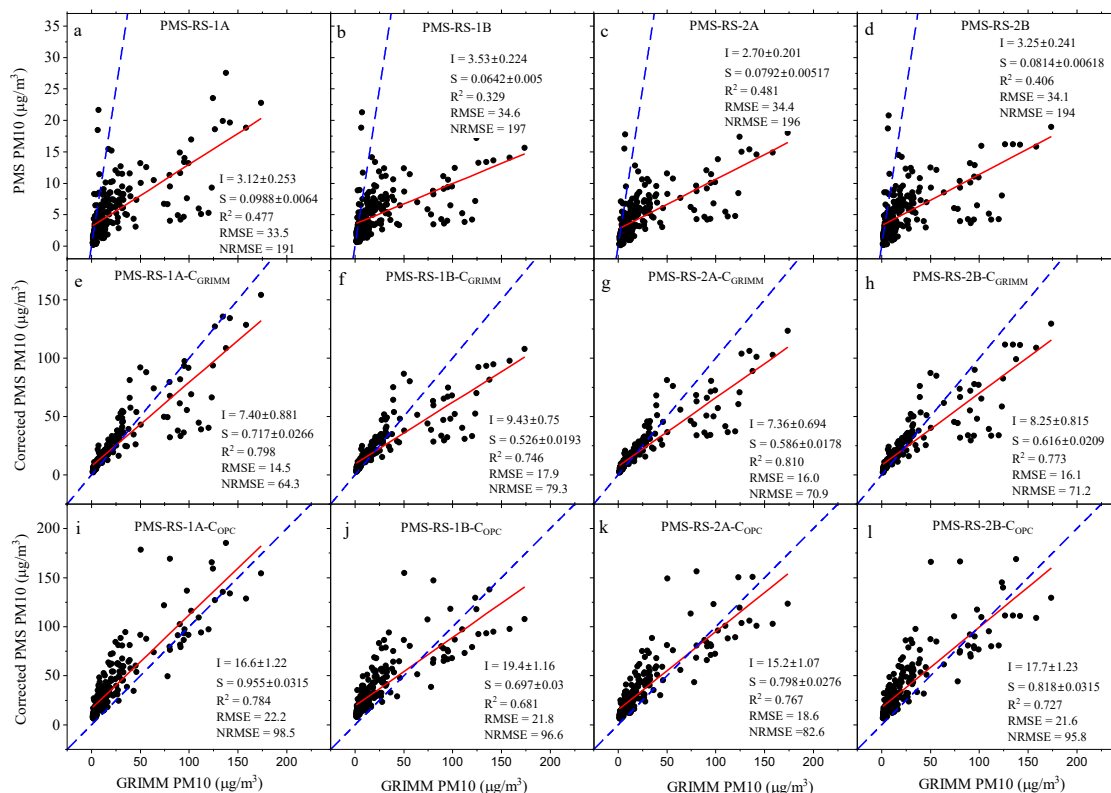
410  
411

### 412 3.4 Correcting PMS data at RS and EQ sites

413 Similar to the HW site, the PMS PM<sub>10</sub> concentration measurements at the RS (Fig. 7, top) exhibited poor-to-moderate  
414 correlation (R<sup>2</sup> between 0.32-0.49, RMSE > 33 μg/m<sup>3</sup>) compared to the research monitor and underestimated the PM<sub>10</sub>  
415 concentrations (slope <0.099). We corrected the raw PMS PM<sub>10</sub> concentration measurements using the PM-ratio-  
416 based correction factors obtained from the HW site and the PM<sub>2.5</sub>/PM<sub>10</sub> ratio from the GRIMM or the OPC to select  
417 a correction factor for each of the six PM<sub>2.5</sub>/PM<sub>10</sub> bins. Using the GRIMM provided ratios, Figure 7 (middle) shows  
418 that at the RS, after PM-ratio-based correction of the PM<sub>10</sub> measurements, the correlation for all the PMS sensors  
419 improved significantly (R<sup>2</sup> > 0.77) and the RMSEs decreased (< 18 μg/m<sup>3</sup>). The R<sup>2</sup> varied between 0.773-0.810, and  
420 the slopes varied between 0.526-0.717. The intercept was a little higher (7-10 μg/m<sup>3</sup>) than the EPA suggested guideline  
421 for low-cost PM<sub>2.5</sub> sensors. All the PMS sensors at RS were freshly deployed and were all mounted on the east side  
422 of a small building. These sensors exhibited good inter-sensor correlation (Fig. S4, R<sup>2</sup> > 0.97, slope > 0.77) and  
423 therefore exhibited very similar improvement all the sensors using the PM-ratio-based correction. The correlations  
424 between PMS PM<sub>10</sub> and GRIMM PM<sub>10</sub> concentrations were also good (R<sup>2</sup>>0.7) when considering PM<sub>10</sub> < 50 μg/m<sup>3</sup>



425 (Fig. S8 vs. Fig. S9), indicating that PM-ratio-based correction factors are applicable during more typical ambient  
 426 levels of PM<sub>10</sub> (without dust events).  
 427



428  
 429  
 430 **Figure 7:** (Top: a, b, c, and d) Uncorrected PMS PM<sub>10</sub> concentration vs. GRIMM PM<sub>10</sub> concentration at RS the site. (Middle: e, f,  
 431 g, and h) Corrected PM<sub>10</sub> concentrations using the PM-ratio-based correction factors developed at HW and the PM<sub>2.5</sub>/PM<sub>10</sub> ratios  
 432 provided by the GRIMM at the RS. (Bottom: i, j, k, and l) Corrected PM<sub>10</sub> concentrations using the PM-ratio-based correction  
 433 factors developed at HW and the PM<sub>2.5</sub>/PM<sub>10</sub> ratios provided by the OPC-RS at the RS. The solid red line represents the linear fit  
 434 and the blue dash line represents the 1:1 line. The plots include measurements recorded between 04/18/2022 – 04/30/2022. I:  
 435 intercept; S: slope. The RMSE and NRMSE has units µg/m<sup>3</sup> and %, respectively.

436  
 437 Figure 7 (bottom) illustrates a similar strategy at the RS site but using the OPC-RS to provide the PM<sub>2.5</sub>/PM<sub>10</sub> ratio. It  
 438 also shows that the correlation for PMS sensors improved after applying the PM-ratio-based correction using the OPC-  
 439 RS for the ratio (R<sup>2</sup> = 0.681 - 0.784). After correction, the slope also increased and varied between 0.589-0.813. The  
 440 corrected RMSE (18.6 – 22.2 µg/m<sup>3</sup>) and intercept (15.2-19.4 µg/m<sup>3</sup>) were somewhat higher than that observed when  
 441 using GRIMM-reported PM ratios (Fig. 7 (middle)). From Figure 7 (bottom), the PM-ratio-based corrected PMS PM<sub>10</sub>  
 442 concentration for PM<sub>10</sub> < 50 µg/m<sup>3</sup> was always above the 1:1 line, i.e., the PMS PM<sub>10</sub> concentration was overestimated.  
 443 The OPC-RS efficiency in counting particles smaller than 0.8 µm is lower than the GRIMM (Bezantakos et al., 2018;  
 444 Sousan et al., 2016), and therefore underestimates PM<sub>2.5</sub> mass. Figure S5 also illustrates this overestimation in our

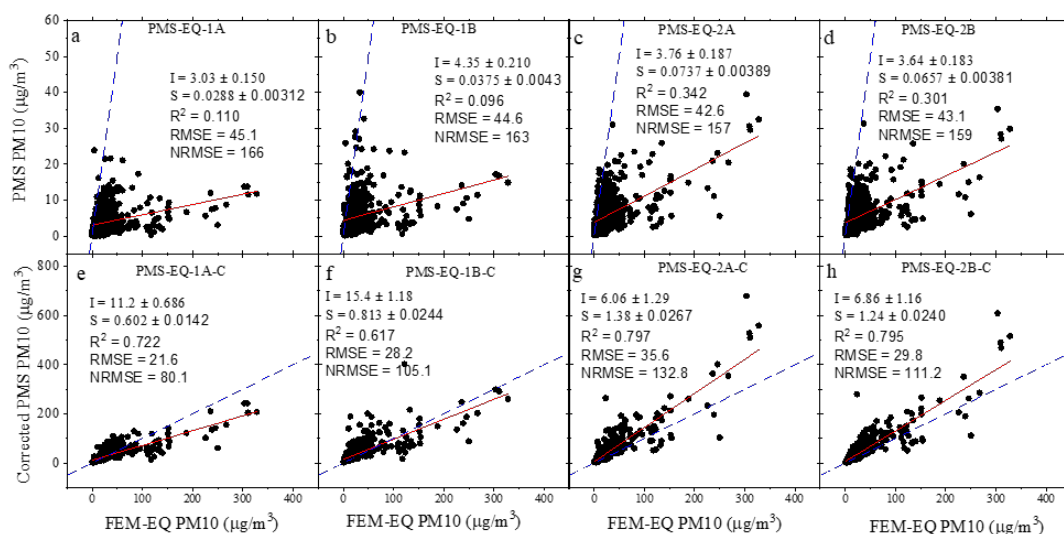


445 study, where for low  $PM_{2.5}$  and  $PM_{10}$  concentrations (90% of the measurements when  $PM_{2.5} < 12 \mu\text{g}/\text{m}^3$  and  $PM_{10} <$   
446  $40 \mu\text{g}/\text{m}^3$ ) the OPC-RS underestimated the  $PM_{2.5}$  mass compared to the GRIMM, although the OPC-RS  $PM_{10}$   
447 concentrations were similar to those of the GRIMM. The underestimated  $PM_{2.5}$  measurements from the OPC affected  
448 the  $PM_{2.5}/PM_{10}$  ratios, which for the OPC-RS remained lower than those reported by the GRIMM (Fig. S6). The  
449 magnitude of the PM-ratio-based correction factors (Fig. 6) was inversely related to the  $PM_{2.5}/PM_{10}$  ratio. Since the  
450 OPC-RS reported ratios were always low, the corrected  $PM_{10}$  measurements below  $50 \mu\text{g}/\text{m}^3$  were overestimated (Fig  
451 S10).

452

453 At the EQ site, we used the  $PM_{2.5}/PM_{10}$  ratios from FEM measurements at the EQ site coupled with the PM-ratio-  
454 based correction factors developed at the HW site to correct the PMS  $PM_{10}$  concentrations from sensors located near  
455 the EQ site. Correcting the PMS  $PM_{10}$  concentrations using this approach did improve the correlation with FEM-EQ  
456 (Fig. 8). Before the correction, all the PMS sensors has poor correlation with the FEM ( $R^2 < 0.342$  and slope  $< 0.0737$ ).  
457 The  $R^2$  improved to 0.617 - 0.797, and the slope increased to 0.602-1.38 after PM-ratio-based correction. The RMSE  
458 decreased and ranged between 21.5 – 35.6  $\mu\text{g}/\text{m}^3$ . The intercept increased and varied between 6.06-15.4. The sensors  
459 at this site showed moderate inter-sensor correlation (Fig. S7), which was expected as these sensors were not  
460 collocated. The different correlations with respect to FEM-EQ for the two PurpleAir II were also expected as these  
461 sensors were not collocated with the FEM-EQ.

462



463

464

465 **Figure 8:** (top: a, b, c, and d) Uncorrected PMS  $PM_{10}$  concentration vs. FEM-EQ  $PM_{10}$  concentrations at the EQ site. (bottom: e,  
466 f, g, and h) Corrected  $PM_{10}$  concentrations using the correction factors developed at HW and the  $PM_{2.5}/PM_{10}$  ratios calculated using  
467 FEM-EQ  $PM_{10}$  and  $PM_{2.5}$  concentrations. The solid red line represents the linear fit and the blue dash line represents the 1:1 line.  
468 The plots include measurements recorded between 04/1/2022 – 04/30/2022. I: intercept; S: slope. The RMSE and NRMSE has  
469 units  $\mu\text{g}/\text{m}^3$  and %, respectively.

470



#### 471 **4 Limitations**

472 This study has several limitations. The sensor's performance was evaluated for a month-long period in April 2022 and  
473 focused primarily on dust events, which commonly occur during this month. Understanding the OPC-N3 performance  
474 and whether using a  $PM_{2.5}/PM_{10}$  ratio-based correction could improve correction factors for PMS sensors in other  
475 seasons and under different environmental conditions, like, wildfires, cold air pools, etc., would require a longer period  
476 of evaluation. This study used four PMS5003 sensors at the HW site and unlike the RS site, the sensors at HW were  
477 deployed at different times. These sensors showed moderate inter-sensor correlation, suggesting the need for further  
478 investigation of sensor age, sensor siting for  $PM_{10}$  measurements, and potentially recalibration. This study occurred  
479 in an arid region, with RH generally less than 60%. This study did not find a significant improvement by adding RH  
480 to a calibration model between the OPC-N3 and the FEM. However, the applicability of this study's results to other,  
481 more humid, regions would need to be evaluated. The correction factors derived in this study used an average of three  
482 co-located PMS sensor measurements at a single site. In absence of detailed information about ambient particle  
483 properties, this study used default constant density for all the size-bins for OPC-N3. The Alphasense OPC-N3 allows  
484 the user to change the size-bin specific density for better estimates of  $PM_{10}$ , and if size-bin density and refractive index  
485 were available, the OPC measurements could potentially be improved. Our proposed PM-ratio-based calibration  
486 method relies on local measurements of the  $PM_{2.5}/PM_{10}$  ratio. This requires FEM or other accurate measurements of  
487  $PM_{2.5}$  and  $PM_{10}$  concentration, and the needed spatial distribution of these accurate  $PM_{2.5}$  and  $PM_{10}$  concentrations  
488 would need to be determined.

489

#### 490 **5 Conclusions**

491 This study evaluated the performance of Alphasense OPC-N3  $PM_{10}$  measurements compared to FEM and GRIMM  
492 measurements during multiple dust events at two locations (HW and RS). The OPC-N3 tracked all the dust events at  
493 the two locations and exhibited a strong correlation with reference measurements ( $R^2 = 0.865 - 0.937$ ), RMSE of 12.4-  
494 17.7  $\mu\text{g}/\text{m}^3$ , and NRMSE of 53.5 - 100 %. Uncorrected PMS5003  $PM_{10}$  measurements showed poor to moderate  
495 correlation ( $R^2 < 0.49$ ) with the reference/research monitors at three locations (HW, RS, and EQ), with a RMSE of  
496 33-45  $\mu\text{g}/\text{m}^3$  and a NRMSE of 145-197 %. The PMS measurements severely underestimated the  $PM_{10}$  concentrations  
497 (slope  $< 0.099$ ). We evaluated a PM-ratio-based correction method to improve estimates of  $PM_{10}$  concentration from  
498 PMS sensors. After applying this method, PMS  $PM_{10}$  concentrations correlated reasonably well with FEM  
499 measurements ( $R^2 > 0.63$ ) and GRIMM measurements ( $R^2 > 0.76$ ), the RMSE decreased to 15-25  $\mu\text{g}/\text{m}^3$  and NRMSE  
500 decreased to 64 - 132 %. Our results suggest that it may be possible to leverage measurements from existing networks  
501 relying on low-cost  $PM_{2.5}$  sensors to obtain better resolved spatial estimates of  $PM_{10}$  concentration using a combination  
502 of PMS sensors and measurements of  $PM_{2.5}$  and  $PM_{10}$ , such as those provided by FEMs, research-grade  
503 instrumentation, or the OPC-N3.

504



505 **Data Availability:**

506 The raw and processed data used in the manuscript can be found at: <https://doi.org/10.7278/S50d-xbns-3ge3>

507 **Authors Contribution:**

508 KEK and KK conceptualized the research, collected, and analysed the data. KK developed the original draft and KEK  
509 reviewed the original draft. KK provided the supervision and acquired the funding.

510 **Competing interests:**

511 Dr. Kerry Kelly has a financial interest in the company Tellus Networked Solutions, LCC, which commercializes  
512 solutions for environmental monitoring. Their technology was not used as part of this work.  
513

514 **Acknowledgements:**

515 This material is based upon work supported by the National Science Foundation under Grant No. 2012091  
516 Collaborative Research Network Cluster: Dust in the Critical Zone and under Grant No. 2228600 CIVIC-PG:  
517 TRACK A: Community Resilience through Engaging, Actionable, Timely, High-Resolution Air Quality  
518 Information (CREATE-AQI). Thanks to PurpleAir for donating two PAAIs to the project.

519 **References:**

- 520 Akinwumiju, A. S., Ajisafe, T., and Adelodun, A. A.: Airborne Particulate Matter Pollution in Akure Metro City,  
521 Southwestern Nigeria, West Africa: Attribution and Meteorological Influence, *Journal of Geovisualization and Spatial*  
522 *Analysis*, 5, 11, <https://doi.org/10.1007/s41651-021-00079-6>, 2021.
- 523 Alhasa, K., Mohd Nadzir, M., Olalekan, P., Latif, M., Yusup, Y., Iqbal Faruque, M., Ahamad, F., Abd. Hamid, H.,  
524 Aiyub, K., Md Ali, S., Khan, M., Abu Samah, A., Yusuff, I., Othman, M., Tengku Hassim, T., and Ezani, N.:  
525 Calibration Model of a Low-Cost Air Quality Sensor Using an Adaptive Neuro-Fuzzy Inference System, *Sensors*, 18,  
526 4380, <https://doi.org/10.3390/s18124380>, 2018.
- 527 WHO: [https://www.who.int/news-room/fact-sheets/detail/ambient-\(outdoor\)-air-quality-and-health](https://www.who.int/news-room/fact-sheets/detail/ambient-(outdoor)-air-quality-and-health), last access: 5  
528 October 2022.
- 529 Ardon-Dryer, K. and Kelley, M. C.: Particle size distribution and particulate matter concentrations during synoptic  
530 and convective dust events in West Texas, *Atmos Chem Phys*, 22, 9161–9173, [https://doi.org/10.5194/acp-22-9161-](https://doi.org/10.5194/acp-22-9161-2022)  
531 [2022](https://doi.org/10.5194/acp-22-9161-2022), 2022.
- 532 Bächler, P., Szabadi, J., Meyer, J., and Dittler, A.: Simultaneous measurement of spatially resolved particle emissions  
533 in a pilot plant scale baghouse filter applying distributed low-cost particulate matter sensors, *J Aerosol Sci*, 150,  
534 <https://doi.org/10.1016/j.jaerosci.2020.105644>, 2020.



- 535 Badura, M., Batog, P., Drzeniecka-Osiadacz, A., and Modzel, P.: Evaluation of low-cost sensors for ambient PM<sub>2.5</sub>  
536 monitoring, *J Sens*, 2018, <https://doi.org/10.1155/2018/5096540>, 2018.
- 537 Bezantakos, S., Schmidt-Ott, F., and Biskos, G.: Performance evaluation of the cost-effective and lightweight  
538 Alphasense optical particle counter for use onboard unmanned aerial vehicles, *Aerosol Science and Technology*, 52,  
539 385–392, <https://doi.org/10.1080/02786826.2017.1412394>, 2018.
- 540 Bi, J., Wildani, A., Chang, H. H., and Liu, Y.: Incorporating Low-Cost Sensor Measurements into High-Resolution  
541 PM<sub>2.5</sub> Modeling at a Large Spatial Scale, *Environ Sci Technol*, 54, 2152–2162,  
542 <https://doi.org/10.1021/acs.est.9b06046>, 2020.
- 543 Bílek, J., Bílek, O., Maršolek, P., and Buček, P.: Ambient air quality measurement with low-cost optical and  
544 electrochemical sensors: An evaluation of continuous year-long operation, *Environments - MDPI*, 8,  
545 <https://doi.org/10.3390/environments8110114>, 2021.
- 546 Bogan, M., Al, B., Kul, S., Zengin, S., Oktay, M., Sabak, M., Gümüşboğa, H., and Bayram, H.: The effects of desert  
547 dust storms, air pollution, and temperature on morbidity due to spontaneous abortions and toxemia of pregnancy: 5-  
548 year analysis, *Int J Biometeorol*, 65, 1733–1739, <https://doi.org/10.1007/s00484-021-02127-8>, 2021.
- 549 Bousiotis, D., Singh, A., Haugen, M., Beddows, D. C. S., Diez, S., Murphy, K. L., Edwards, P. M., Boies, A., Harrison,  
550 R. M., and Pope, F. D.: Assessing the sources of particles at an urban background site using both regulatory  
551 instruments and low-cost sensors – a comparative study, *Atmos Meas Tech*, 14, 4139–4155,  
552 <https://doi.org/10.5194/amt-14-4139-2021>, 2021.
- 553 Cai, H., Yang, Y., Luo, W., and Chen, Q.: City-level variations in aerosol optical properties and aerosol type  
554 identification derived from long-term MODIS/Aqua observations in the Sichuan Basin, China, *Urban Clim*, 38,  
555 100886, <https://doi.org/10.1016/j.uclim.2021.100886>, 2021.
- 556 Caplin, A., Ghandehari, M., Lim, C., Glimcher, P., and Thurston, G.: Advancing environmental exposure assessment  
557 science to benefit society, *Nat Commun*, 10, 1236, <https://doi.org/10.1038/s41467-019-09155-4>, 2019.
- 558 Caubel, J. J., Cados, T. E., Preble, C. v., and Kirchstetter, T. W.: A Distributed Network of 100 Black Carbon Sensors  
559 for 100 Days of Air Quality Monitoring in West Oakland, California, *Environ Sci Technol*, 53, 7564–7573,  
560 <https://doi.org/10.1021/acs.est.9b00282>, 2019.
- 561 Chakravarty, K., Vincent, V., Vellore, R., Srivastava, A. K., Rastogi, A., and Soni, V. K.: Revisiting Andhi in northern  
562 India: A case study of severe dust-storm over the urban megacity of New Delhi, *Urban Clim*, 37, 100825,  
563 <https://doi.org/10.1016/j.uclim.2021.100825>, 2021.
- 564 Chu, M. D. T., Gillooly, S. E., Levy, J. I., Vallarino, J., Reyna, L. N., Cedeño Laurent, J. G., Coull, B. A., and  
565 Adamkiewicz, G.: Real-time indoor PM<sub>2.5</sub> monitoring in an urban cohort: Implications for exposure disparities and  
566 source control, *Environ Res*, 193, <https://doi.org/10.1016/j.envres.2020.110561>, 2021.
- 567 Clifford, H. M., Spaulding, N. E., Kurbatov, A. v., More, A., Korotkikh, E. v., Sneed, S. B., Handley, M., Maasch, K.  
568 A., Loveluck, C. P., Chaplin, J., McCormick, M., and Mayewski, P. A.: A 2000 Year Saharan Dust Event Proxy  
569 Record from an Ice Core in the European Alps, *Journal of Geophysical Research: Atmospheres*, 124, 12882–12900,  
570 <https://doi.org/10.1029/2019JD030725>, 2019.



- 571 Crilley, L. R., Shaw, M., Pound, R., Kramer, L. J., Price, R., Young, S., Lewis, A. C., and Pope, F. D.: Evaluation of  
572 a low-cost optical particle counter (Alphasense OPC-N2) for ambient air monitoring, *Atmos Meas Tech*, 11, 709–720,  
573 <https://doi.org/10.5194/amt-11-709-2018>, 2018.
- 574 Dastoorpoor, M., Idani, E., Goudarzi, G., and Khanjani, N.: Acute effects of air pollution on spontaneous abortion,  
575 premature delivery, and stillbirth in Ahvaz, Iran: a time-series study, *Environmental Science and Pollution Research*,  
576 25, 5447–5458, <https://doi.org/10.1007/s11356-017-0692-9>, 2018.
- 577 Met One Technical Bulletin BAM-1020 Detection Limit: [https://metone.com/wp-content/uploads/2019/04/bam-](https://metone.com/wp-content/uploads/2019/04/bam-1020_detection_limit.pdf)  
578 [1020\\_detection\\_limit.pdf](https://metone.com/wp-content/uploads/2019/04/bam-1020_detection_limit.pdf), last access: 5 October 2022.
- 579 Diokhane, A. M., Jenkins, G. S., Manga, N., Drame, M. S., and Mbodji, B.: Linkages between observed, modeled  
580 Saharan dust loading and meningitis in Senegal during 2012 and 2013, *Int J Biometeorol*, 60, 557–575,  
581 <https://doi.org/10.1007/s00484-015-1051-5>, 2016.
- 582 Dubey, R., Patra, A. K., Joshi, J., Blankenberg, D., Kolluru, S. S. R., Madhu, B., and Raval, S.: Evaluation of low-  
583 cost particulate matter sensors OPC N2 and PM Nova for aerosol monitoring, *Atmos Pollut Res*, 13,  
584 <https://doi.org/10.1016/j.apr.2022.101335>, 2022a.
- 585 Dubey, R., Patra, A. K., Joshi, J., Blankenberg, D., and Nazneen: Evaluation of vertical and horizontal distribution of  
586 particulate matter near an urban roadway using an unmanned aerial vehicle, *Science of the Total Environment*, 836,  
587 <https://doi.org/10.1016/j.scitotenv.2022.155600>, 2022b.
- 588 Duvall, R. M., Hagler, G. S. W., Clements, A. L., Benedict, K., Barkjohn, K., Kilaru, V., Hanley, T., Watkins, N.,  
589 Kaufman, A., Kamal, A., Reece, S., Fransioli, P., Gerboles, M., Gillerman, G., Habre, R., Hannigan, M., Ning, Z.,  
590 Papapostolou, V., Pope, R., Quintana, P. J. E., and Lam Snyder, J.: Deliberating Performance Targets: Follow-on  
591 workshop discussing PM10, NO2, CO, and SO2 air sensor targets, in: *Atmospheric Environment*,  
592 <https://doi.org/10.1016/j.atmosenv.2020.118099>, 2021.
- 593 EPA: <https://www.epa.gov/outdoor-air-quality-data/interactive-map-air-quality-monitors>, last access: 5 October  
594 2022.
- 595 USA EPA: [https://aqsw.epa.gov/aqsweb/airdata/download\\_files.html](https://aqsw.epa.gov/aqsweb/airdata/download_files.html), last access: 4 October 2022.
- 596 Feenstra, B., Papapostolou, V., Hasheminassab, S., Zhang, H., Boghossian, B. der, Cocker, D., and Polidori, A.:  
597 Performance evaluation of twelve low-cost PM2.5 sensors at an ambient air monitoring site, *Atmos Environ*, 216,  
598 <https://doi.org/10.1016/j.atmosenv.2019.116946>, 2019.
- 599 Gomes, J., Esteves, H., and Rente, L.: Influence of an Extreme Saharan Dust Event on the Air Quality of the West  
600 Region of Portugal, *Gases*, 2, 74–84, <https://doi.org/10.3390/gases2030005>, 2022.
- 601 Goudie, A. S.: Desert dust and human health disorders, *Environ Int*, 63, 101–113,  
602 <https://doi.org/10.1016/j.envint.2013.10.011>, 2014.
- 603 Hahnenberger, M. and Nicoll, K.: Meteorological characteristics of dust storm events in the eastern Great Basin of  
604 Utah, U.S.A., *Atmos Environ*, 60, 601–612, <https://doi.org/10.1016/J.ATMOSENV.2012.06.029>, 2012.
- 605 Harr, L., Sinsel, T., Simon, H., Konter, O., Dreiseitl, D., Schulz, P., and Esper, J.: PM2.5 exposure differences between  
606 children and adults, *Urban Clim*, 44, <https://doi.org/10.1016/j.uclim.2022.101198>, 2022a.



- 607 Harr, L., Sinsel, T., Simon, H., and Esper, J.: Seasonal Changes in Urban PM<sub>2.5</sub> Hotspots and Sources from Low-  
608 Cost Sensors, *Atmosphere (Basel)*, 13, <https://doi.org/10.3390/atmos13050694>, 2022b.
- 609 He, M., Kuerbanjiang, N., and Dhaniyala, S.: Performance characteristics of the low-cost Plantower PMS optical  
610 sensor, *Aerosol Science and Technology*, 54, 232–241, <https://doi.org/10.1080/02786826.2019.1696015>, 2020.
- 611 Huang, J., Ji, M., Xie, Y., Wang, S., He, Y., and Ran, J.: Global semi-arid climate change over last 60 years, *Clim  
612 Dyn*, 46, 1131–1150, <https://doi.org/10.1007/s00382-015-2636-8>, 2016.
- 613 Imami, A. D., Drijeana, Villegas, E. R., and McFiggans, G.: Evaluation of Alphasense OPC-N2 sensor for PM<sub>10</sub>  
614 measurement in the North Jakarta, *ASEAN Engineering Journal*, 12, 243–248,  
615 <https://doi.org/10.11113/aej.V12.17853>, 2022.
- 616 Jayaratne, E. R., Johnson, G. R., McGarry, P., Cheung, H. C., and Morawska, L.: Characteristics of airborne ultrafine  
617 and coarse particles during the Australian dust storm of 23 September 2009, *Atmos Environ*, 45, 3996–4001,  
618 <https://doi.org/10.1016/j.atmosenv.2011.04.059>, 2011.
- 619 Jones, B. A.: After the Dust Settles: The Infant Health Impacts of Dust Storms, *J Assoc Environ Resour Econ*, 7,  
620 1005–1032, <https://doi.org/10.1086/710242>, 2020.
- 621 Kaliszewski, M., Włodarski, M., Młyńczak, J., and Kopczyński, K.: Comparison of low-cost particulate matter sensors  
622 for indoor air monitoring during covid-19 lockdown, *Sensors (Switzerland)*, 20, 1–17,  
623 <https://doi.org/10.3390/s20247290>, 2020.
- 624 Keet, C. A., Keller, J. P., and Peng, R. D.: Long-Term Coarse Particulate Matter Exposure Is Associated with Asthma  
625 among Children in Medicaid, *Am J Respir Crit Care Med*, 197, 737–746, <https://doi.org/10.1164/rccm.201706-1267OC>, 2018.
- 627 Kelly, K. E., Xing, W. W., Sayahi, T., Mitchell, L., Becnel, T., Gaillardon, P.-E., Meyer, M., and Whitaker, R. T.:  
628 Community-Based Measurements Reveal Unseen Differences during Air Pollution Episodes, *Environ Sci Technol*,  
629 55, 120–128, <https://doi.org/10.1021/acs.est.0c02341>, 2021.
- 630 Kosmopoulos, G., Salamalikis, V., Pandis, S. N., Yannopoulos, P., Bloutsos, A. A., and Kazantzidis, A.: Low-cost  
631 sensors for measuring airborne particulate matter: Field evaluation and calibration at a South-Eastern European site,  
632 *Science of the Total Environment*, 748, <https://doi.org/10.1016/j.scitotenv.2020.141396>, 2020.
- 633 Kumar, S., Singh, A., Srivastava, A. K., Sahu, S. K., Hooda, R. K., Dumka, U. C., and Pathak, V.: Long-term change  
634 in aerosol characteristics over Indo-Gangetic Basin: How significant is the impact of emerging anthropogenic  
635 activities?, *Urban Clim*, 38, 100880, <https://doi.org/10.1016/j.uclim.2021.100880>, 2021.
- 636 Kuula, J., Mäkelä, T., Aurela, M., Teinilä, K., Varjonen, S., González, Ó., and Timonen, H.: Laboratory evaluation of  
637 particle-size selectivity of optical low-cost particulate matter sensors, *Atmos Meas Tech*, 13, 2413–2423,  
638 <https://doi.org/10.5194/amt-13-2413-2020>, 2020.
- 639 Lim, C. C., Kim, H., Vilcassim, M. J. R., Thurston, G. D., Gordon, T., Chen, L.-C., Lee, K., Heimbinder, M., and  
640 Kim, S.-Y.: Mapping urban air quality using mobile sampling with low-cost sensors and machine learning in Seoul,  
641 South Korea, *Environ Int*, 131, 105022, <https://doi.org/10.1016/j.envint.2019.105022>, 2019.



- 642 Liu, L., Duan, Y., Li, L., Xu, L., Yang, Y., and Cu, X.: Spatiotemporal trends of PM<sub>2.5</sub> concentrations and typical  
643 regional pollutant transport during 2015–2018 in China, *Urban Clim*, 34, 100710,  
644 <https://doi.org/10.1016/j.uclim.2020.100710>, 2020.
- 645 Mallet, M., Tulet, P., Serça, D., Solmon, F., Dubovik, O., Pelon, J., Pont, V., and Thouron, O.: Impact of dust aerosols  
646 on the radiative budget, surface heat fluxes, heating rate profiles and convective activity over West Africa during  
647 March 2006, *Atmos Chem Phys*, 9, 7143–7160, <https://doi.org/10.5194/acp-9-7143-2009>, 2009.
- 648 Masic, A., Bibic, D., Pikula, B., Blazevic, A., Huremovic, J., and Zero, S.: Evaluation of optical particulate matter  
649 sensors under realistic conditions of strong and mild urban pollution, *Atmos Meas Tech*, 13, 6427–6443,  
650 <https://doi.org/10.5194/amt-13-6427-2020>, 2020.
- 651 Mei, H., Han, P., Wang, Y., Zeng, N., Liu, D., Cai, Q., Deng, Z., Wang, Y., Pan, Y., and Tang, X.: Field evaluation  
652 of low-cost particulate matter sensors in Beijing, *Sensors (Switzerland)*, 20, 1–17, <https://doi.org/10.3390/s20164381>,  
653 2020.
- 654 Mohd Nadzir, M. S., Ooi, M. C. G., Alhasa, K. M., Bakar, M. A. A., Mohtar, A. A. A., Nor, M. F. F. M., Latif, M. T.,  
655 Hamid, H. H. A., Ali, S. H. M., Ariff, N. M., Anuar, J., Ahamad, F., Azhari, A., Hanif, N. M., Subhi, M. A., Othman,  
656 M., and Nor, M. Z. M.: The Impact of Movement Control Order (MCO) during Pandemic COVID-19 on Local Air  
657 Quality in an Urban Area of Klang Valley, Malaysia, *Aerosol Air Qual Res*, 20, 1237–1248,  
658 <https://doi.org/10.4209/aaqr.2020.04.0163>, 2020.
- 659 Mukherjee, A., Stanton, L. G., Graham, A. R., and Roberts, P. T.: Assessing the utility of low-cost particulate matter  
660 sensors over a 12-week period in the Cuyama valley of California, *Sensors (Switzerland)*, 17,  
661 <https://doi.org/10.3390/s17081805>, 2017.
- 662 Nor, N. S. M., Yip, C. W., Ibrahim, N., Jaafar, M. H., Rashid, Z. Z., Mustafa, N., Hamid, H. H. A., Chandru, K., Latif,  
663 M. T., Saw, P. E., Lin, C. Y., Alhasa, K. M., Hashim, J. H., and Nadzir, M. S. M.: Particulate matter (PM<sub>2.5</sub>) as a  
664 potential SARS-CoV-2 carrier, *Sci Rep*, 11, 2508, <https://doi.org/10.1038/s41598-021-81935-9>, 2021.
- 665 Ouimette, J. R., Malm, W. C., Schichtel, B. A., Sheridan, P. J., Andrews, E., Ogren, J. A., and Arnott, W. P.:  
666 Evaluating the PurpleAir monitor as an aerosol light scattering instrument, *Atmos Meas Tech*, 15, 655–676,  
667 <https://doi.org/10.5194/amt-15-655-2022>, 2022.
- 668 Perry, K. D., Crosman, E. T., and Hoch, S. W.: Results of the Great Salt Lake Dust Plume Study (2016–2018), 2019.
- 669 Pope, F. D., Gatari, M., Ng'ang'a, D., Poynter, A., and Blake, R.: Airborne particulate matter monitoring in Kenya  
670 using calibrated low-cost sensors, *Atmos Chem Phys*, 18, 15403–15418, <https://doi.org/10.5194/acp-18-15403-2018>,  
671 2018.
- 672 Rachele M. Duvall, Andrea L. Clements, Gayle Hagler, Ali Kamal, Vasu Kilaru, Laura Goodman, Samuel Frederick,  
673 Karoline K. (Johnson) Barkjohn, Ian VonWal, Danny Greene, and Tim Dye: Performance Testing Protocols, Metrics,  
674 and Target Values for Fine Particulate Matter Air Sensors: Use in Ambient, Outdoor, Fixed Site, Non-Regulatory  
675 Supplemental and Informational Monitoring Applications, 2021.
- 676 Runström Eden, G., Tinnerberg, H., Rosell, L., Möller, R., Almstrand, A. C., and Bredberg, A.: Exploring Methods  
677 for Surveillance of Occupational Exposure from Additive Manufacturing in Four Different Industrial Facilities, *Ann  
678 Work Expo Health*, 66, 163–177, <https://doi.org/10.1093/annweh/wxab070>, 2022.



- 679 Samad, A., Mimiaga, F. E. M., Laquai, B., and Vogt, U.: Investigating a low-cost dryer designed for low-cost PM  
680 sensors measuring ambient air quality, *Sensors (Switzerland)*, 21, 1–18, <https://doi.org/10.3390/s21030804>, 2021.
- 681 Sayahi, T., Butterfield, A., and Kelly, K. E.: Long-term field evaluation of the Plantower PMS low-cost particulate  
682 matter sensors, *Environmental Pollution*, 245, 932–940, <https://doi.org/10.1016/j.envpol.2018.11.065>, 2019.
- 683 Schweitzer, M. D., Calzadilla, A. S., Salamo, O., Sharifi, A., Kumar, N., Holt, G., Campos, M., and Mirsaedi, M.:  
684 Lung health in era of climate change and dust storms, *Environ Res*, 163, 36–42,  
685 <https://doi.org/10.1016/j.envres.2018.02.001>, 2018.
- 686 Sousan, S., Koehler, K., Hallett, L., and Peters, T. M.: Evaluation of the Alphasense optical particle counter (OPC-  
687 N2) and the Grimm portable aerosol spectrometer (PAS-1.108), *Aerosol Science and Technology*, 50, 1352–1365,  
688 <https://doi.org/10.1080/02786826.2016.1232859>, 2016.
- 689 Sousan, S., Regmi, S., and Park, Y. M.: Laboratory evaluation of low-cost optical particle counters for environmental  
690 and occupational exposures, *Sensors*, 21, <https://doi.org/10.3390/s21124146>, 2021.
- 691 Soy, F. K.: The effects of dust storms on quality of life of allergic patients with or without asthma, *The Turkish Journal*  
692 *of Ear Nose and Throat*, 26, 19–27, <https://doi.org/10.5606/kbbihtisas.2016.56254>, 2016.
- 693 Speranza, A., Caggiano, R., Margiotta, S., and Trippetta, S.: A novel approach to comparing simultaneous size-  
694 segregated particulate matter (PM) concentration ratios by means of a dedicated triangular diagram using the Agri  
695 Valley PM measurements as an example, *Natural Hazards and Earth System Sciences*, 14, 2727–2733,  
696 <https://doi.org/10.5194/nhess-14-2727-2014>, 2014.
- 697 Sugimoto, N., Shimizu, A., Matsui, I., and Nishikawa, M.: A method for estimating the fraction of mineral dust in  
698 particulate matter using PM<sub>2.5</sub>-to-PM<sub>10</sub> ratios, *Particology*, 28, 114–120,  
699 <https://doi.org/10.1016/j.partic.2015.09.005>, 2016.
- 700 Tagle, M., Rojas, F., Reyes, F., Vásquez, Y., Hallgren, F., Lindén, J., Kolev, D., Watne, Å. K., and Oyola, P.: Field  
701 performance of a low-cost sensor in the monitoring of particulate matter in Santiago, Chile, *Environ Monit Assess*,  
702 192, 171, <https://doi.org/10.1007/s10661-020-8118-4>, 2020.
- 703 Tam, W. W. S., Wong, T. W., Wong, A. H. S., and Hui, D. S. C.: Effect of dust storm events on daily emergency  
704 admissions for respiratory diseases, *Respirology*, 17, 143–148, <https://doi.org/10.1111/j.1440-1843.2011.02056.x>,  
705 2012.
- 706 Alphasense Ltd: <https://www.alphasense.com/wp-content/uploads/2022/09/Alphasense OPC-N3 datasheet.pdf>, last  
707 access: 12 October 2022.
- 708 Tong, D. Q., Wang, J. X. L., Gill, T. E., Lei, H., and Wang, B.: Intensified dust storm activity and Valley fever  
709 infection in the southwestern United States, *Geophys Res Lett*, 44, 4304–4312,  
710 <https://doi.org/10.1002/2017GL073524>, 2017.
- 711 Trianti, S.-M., Samoli, E., Rodopoulou, S., Katsouyanni, K., Papiris, S. A., and Karakatsani, A.: Desert dust outbreaks  
712 and respiratory morbidity in Athens, Greece, *Environmental Health*, 16, 72, [https://doi.org/10.1186/s12940-017-0281-](https://doi.org/10.1186/s12940-017-0281-x)  
713 [x](https://doi.org/10.1186/s12940-017-0281-x), 2017.



- 714 Tryner, J., Mehaffy, J., Miller-Lionberg, D., and Volckens, J.: Effects of aerosol type and simulated aging on  
715 performance of low-cost PM sensors, *J Aerosol Sci*, 150, 105654, <https://doi.org/10.1016/j.jaerosci.2020.105654>,  
716 2020.
- 717 Vogt, M., Schneider, P., Castell, N., and Hamer, P.: Assessment of low-cost particulate matter sensor systems against  
718 optical and gravimetric methods in a field co-location in norway, *Atmosphere (Basel)*, 12,  
719 <https://doi.org/10.3390/atmos12080961>, 2021.
- 720 Williams, A. P., Cook, B. I., and Smerdon, J. E.: Rapid intensification of the emerging southwestern North American  
721 megadrought in 2020–2021, *Nat Clim Chang*, 12, 232–234, <https://doi.org/10.1038/s41558-022-01290-z>, 2022.
- 722 Xu, G., Jiao, L., Zhang, B., Zhao, S., Yuan, M., Gu, Y., Liu, J., and Tang, X.: Spatial and temporal variability of the  
723 PM<sub>2.5</sub>/PM<sub>10</sub> ratio in Wuhan, Central China, *Aerosol Air Qual Res*, 17, 741–751,  
724 <https://doi.org/10.4209/aaqr.2016.09.0406>, 2017.
- 725